Numerical modeling of gravity-driven bubble flows with account of polydispersion

A S Chernyshev and A A Schmidt

Computational Physics Laboratory, Ioffe Institute, Politekhnicheskaya 26, Saint Petersburg, 194021, Russia

E-mail: alexander.tchernyshev@mail.ioffe.ru

Abstract. The present study is focused on the investigation of motion of bubble-liquid medium inside the bubble columns or vertical pipes with account of polydisperse phenomena by the means of numerical simulation. The underlying mathematical model is based on the Euler-Euler approach with interphase interaction described by the momentum and mass transfer between phases, along with the k-ω-SST turbulence model which includes turbulence generation by the bubble motion and bubble path dispersion. Polydispersion is taken into account by the multi-class model with piecewise-constant distribution of bubble sizes per cell. Simulation of downward flow inside the straight vertical pipe resulted in maximum of the bubble void fraction close to the pipe center which is in good correlation with the experimental data. Simulation of multiphase flow inside rectangular bubble column with off-center sparger resulted in vertical bubble-liquid jet which is biased towards nearby wall with the correct prediction of attachment point location.

1. Introduction

Investigations of bubbly flows are of great importance since such flows can be frequently observed in natural phenomena and technological processes. Such investigations involved, for example, the study of the suppression of the bubble formation process, which is important in such facilities as heat exchangers or fuel pipelines and closely related to the cavitation phenomena [1, 2], or dedicated to the optimization of chemical reactors [3]. Direct measurements of the entire flow pattern are not always possible, thus numerical modeling is employed.

Different approaches are used to describe bubble-liquid medium (see, for example, [4]). It is found that two most widely used approaches, the Euler-Euler and the Euler-Lagrange, are suitable for real-scale problems with significant number of bubbles, while with the increase of bubble quantity the latter one becomes more resource demanding.

Treatment of the variation of bubble sizes in the framework of the Euler-Euler approach can be done in a number of ways. The simplest one is to assume that locally all bubbles have same size equals to the Sauter mean diameter [5], which can be used in some problems but fails when bubbles have wide variation in sizes and local size constrain can not be matched. Polydispersion can be implemented in that cases by introducing the population balance equation [6]. Such model provides description of the bubble size variation in each point of space, but due to the integral-differential

nature of the equation the solution procedure became complex. Another approach is a multi-class or multi-size-group (MUSIG) [7, 8] model. This method consists in grouping all bubbles according to their sizes in a number of classes from minimal to maximal size, the number of classes is the same for the entire domain. Mass and momentum conservation equations are formulated and solved for each class of bubbles, with the conservation equations for liquid phase. This model provides unified description of all phases and classes of bubbles with the possibility of simple incorporation inter-phase and class-to-class mass and momentum exchange processes.

The presented work is focused on the improvement of the previously developed Euler-Euler model by incorporation of the polydisperse multi-class approach and conducting simulations for justification of the proposed model and numerical algorithm.

2. Mathematical model

The mathematical model is an extension of the previously developed Euler-Euler model with single-size bubbles [3, 9]. Since N classes are introduced and mass and momentum conservation equations for dispersed and liquid phases will have the following form:

$$\begin{gathered}
\frac{\partial \alpha_{ib}\rho_b^0}{\partial t}+\operatorname{div}\left(\alpha_{ib}\rho_b^0\vec{V}_{ib}\right)=0,\\
\frac{\partial \alpha_{ib}\rho_b^0\vec{V}_{ib}}{\partial t}+\operatorname{div}\left(\alpha_{ib}\rho_b^0\vec{V}_{ib}\vec{V}_{ib}+p\bar{E}\right)=S_{ib},\\
\frac{\partial\left(1-\sum_{i=1}^{N}\alpha_{ib}\right)\rho_l^0}{\partial t}+\operatorname{div}\left(\left(1-\sum_{i=1}^{N}\alpha_{ib}\right)\rho_l^0\vec{V}_l\right)=0,\\
\frac{\partial\left(1-\sum_{i=1}^{N}\alpha_{ib}\right)\rho_l^0\vec{V}_l}{\partial t}+\operatorname{div}\left(\left(1-\sum_{i=1}^{N}\alpha_{ib}\right)\rho_l^0\vec{V}_l\vec{V}_l+p\bar{E}-\bar{\tau}_l\right)=S_l.
\end{gathered} \tag{1}$$

Subscript i for the first two equations of the dispersed phase refers to the i-th class of bubbles, i=1,...,N. This system should be accomplished by conservation equations of number densities per each class:

$$\frac{\partial N_{ib}}{\partial t}+\operatorname{div}\left(N_{ib}\vec{V}_{ib}\right)=0. \tag{2}$$

The initial distribution of bubbles by their sizes in the bulk liquid, or distribution of bubbles at inlet boundaries can be described by Log-Normal or the Rosin-Rammler distributions:

$$\begin{gathered}
\mathrm{LN}:\frac{1}{R\sigma\sqrt{2\pi}}\cdot\exp\left(-\left(\ln\left(R\right)-\mu\right)^2\cdot 0.5\sigma^{-2}\right),\\
\mathrm{RR}:\frac{k}{\lambda}\left(\frac{R}{\lambda}\right)^{k-1}\cdot\exp\left(-\left(R/\lambda\right)^k\right), R\geq 0.
\end{gathered} \tag{3}$$

Mathematical expectations in that distributions are taken equal to most probable bubble size, which can be estimated from the problem set-up parameters or taken from the experimental data. The number of classes N is usually in the range from 5 to 10, and selected on the criteria of converged solution and invariance of the solution from N.

2.1. Turbulence

The *k*-*ω*-SST model is used to describe turbulence:

$$\begin{aligned}&\frac{\partial(\rho_l k)}{\partial t}+\mathrm{div}(\rho_l \vec{V}_l k)\\&=\widetilde{P}-\beta^*\rho_l\omega k+\mathrm{div}\left[(\mu_{lam}+\sigma_k\mu_{turb})\,\mathrm{grad}\,k\right]+\sum_{i=1}^{N}S_{ibk},\\&\frac{\partial(\rho_l \omega)}{\partial t}+\mathrm{div}(\rho_l \vec{V}_l \omega)\\&=\alpha_{k\omega}\frac{\rho_l}{\mu_{turb}}\widetilde{P}-\beta\rho_l\omega^2+\mathrm{div}\left[(\mu_{lam}+\sigma_\omega\mu_{turb})\,\mathrm{grad}\,\omega\right]+2(1-F_1)\rho_l\sigma_{\omega 2}\frac{1}{\omega}\frac{\partial k}{\partial x_i}\frac{\partial \omega}{\partial x_i}+\sum_{i=1}^{N}S_{ib\omega},\end{aligned}\tag{4}$$

with modifications according to the bubble turbulence generation and dissipation terms:

$$S_{ibk}=\frac{3}{8}\frac{C_{iD}}{R_{ib}}\alpha_{ib}\rho_l\left|\vec{V}_{irel}\right|^3,\quad S_{ib\omega}=0.8\frac{k}{\mu_{turb}}S_{ibk}.\tag{5}$$

2.2. Interphase momentum transfer

The Stokesian drag force F_{iD}, lift force F_{iL} and turbulent dispersion force F_{iTD} are included into the momentum transfer equation per each phase:

$$S_{ib}=\alpha_{ib}\rho_b^0\vec{g}+\vec{F}_{iD}+\vec{F}_{iL}+\vec{F}_{iTD},\quad S_l=\left(1-\sum_{i=1}^{N}\alpha_{ib}\right)\rho_l^0\vec{g}-\sum_{i=1}^{N}\left(\vec{F}_{iD}+\vec{F}_{iL}+\vec{F}_{iTD}\right),\tag{6}$$

$$\vec{F}_{iD}=\frac{3\rho_l}{8R_{ib}}C_{iD}\vec{V}_{irel}\left|\vec{V}_{irel}\right|,\vec{V}_{irel}=\vec{V}_l-\vec{V}_{ib},\tag{7}$$

$$\vec{F}_{iL}=C_{iL}\alpha_{ib}\rho_l\vec{V}_{irel}\times\mathrm{rot}\,\vec{V}_l,\tag{8}$$

$$\vec{F}_{iTD}=-1.2C_{iD}\frac{3}{8}\frac{\left|\vec{V}_{irel}\right|}{R_{ib}}\mu^{eff}\nabla\alpha_{ib},\tag{9}$$

expressions for C_{iD} and C_{iL} were taken from [10] and [11], respectively.

3. Numerical method

The numerical method is based on the finite-volume approach and unstructured grids with co-located storage of flow variables. Pressure and velocity are found in separate fashion by modified phase coupled SIMPLE (PC-SIMPLE) algorithm which is based on the original SIMPLE proposed by Patankar [12]. The modified PC-SIMPLE includes only carrier fluid fluxes for pressure correction, since fluxes of dispersed phase are negligibly small due to low density of gas phase. Such assumption makes additional constraint on the bubble volume fraction which should not exceed 20% and is satisfied in the following simulations. A second order accuracy over spatial coordinates provided by TVD schemes and iterative process is realized through the implicit first-order pseudotime marching scheme. Elimination of the effect of mesh skewness is done by the orthogonal correction in calculation of viscous fluxes and curvilinear gradient calculation scheme.

4. Results

4.1. Downward flow in a straight pipe

Simulations of downward bubbly flow inside a vertical straight pipe were carried out according to the conditions mentioned in [13]. Water with immersed air bubbles is supplied to the top end of the

straight vertical pipe with the diameter D=25.4 mm and length L=150D. At the inlet, the superficial liquid velocity V_L=1.25 m/s, superficial gas velocity V_G=0.087 m/s and gas void fraction α=0.067. The most probable bubble size is 2 mm diameter, all bubbles distributed uniformly across inlet area. Experiments were carried out at normal conditions with temperature T=297 K and pressure P=101350 Pa.

Numerical simulations conducted on axisymmetrical geometry with 50 cells across radial coordinate with denser mesh near pipe walls, which provides required resolution of flow gradients. Due to significant difference in density, the effect of gravity was included into the simulation setup which resulted in the buoyant (Archimedean) force. Data was extracted from the radial cross-section which is located at the position z=133D from the inlet location.

The simulation results and experimental data points are presented in the figure 1 and figure 2 – void fraction and velocity distributions, respectively. It can be seen that lift force, which acts along the direction perpendicular to the slip velocity between bubble and liquid, at large distances can significantly alter the profile of bubble concentration, dragging the bubbles toward center of the pipe. Such behavior is a common for downward flows, for upward flows opposite behavior will be observed. Such flow changes can be favored for heat transfer pipelines/heat exchangers, since reduction of bubbles near walls intensified wall-liquid heat transfer. The velocity distribution reaches maximum value close to the center of the pipe, with local maximum near the wall. Such behavior can be explained by taking into the consideration several competitive processes: the Stokesian drag and wall friction forces slow down the flow, while the gravity force accelerates the flow. Due to the drop of the bubble concentration near the wall, impact of the drag force reduces and liquid velocity increases with the formation of the localized velocity peak. All results obtained in simulations are in good agreement with the experimental data.

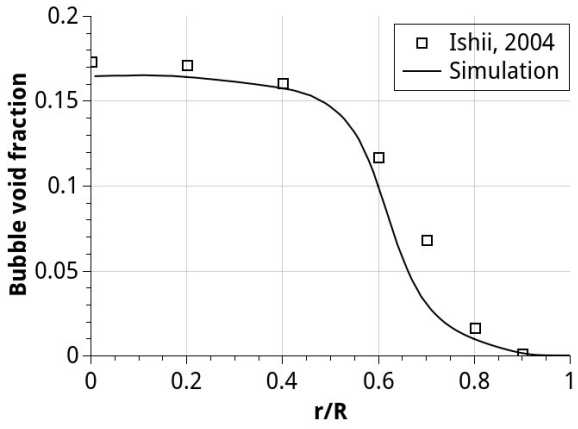

Figure 1. Bubble void fraction distribution at z=133D. Solid line is the simulation, squares are the experimental data [13].

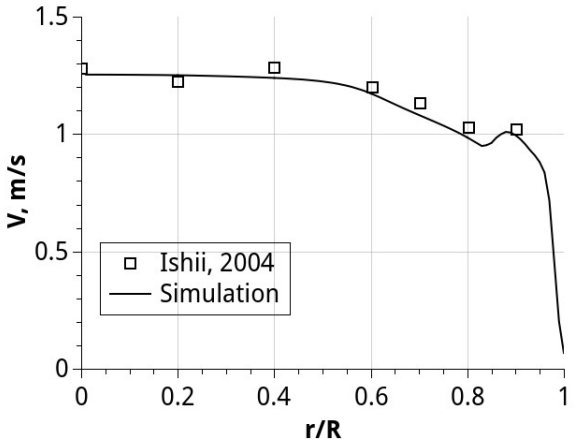

Figure 2. Velocity distribution at z=133D. Solid line is the simulation, squares are the experimental data [13].

4.2. Bubble column reactor

The flow pattern inside a full-scale laboratory bubble column reactor was investigated in [14]. The reactor has parallelepiped shape with dimensions of 500 mm width, 80 mm depth and 1500 mm hight. A bubble injector (sparger) has depth of 80 mm and mounted in the bottom wall at the distance of 160 mm from the left wall. The entire volume of the column is filled by pure water and air bubbles are supplied into the reactor through the sparger with the superficial velocity V_G=0.66 mm/s. The mean

diameter of the initial bubble was taken equal to 2 mm. The experiments were carried out at normal conditions with room temperature T=297 K and pressure P=101350 Pa.

The hexahedral orthogonal mesh was constructed with dense mesh towards walls to provide adequate resolution of boundary layers. The top boundary condition was assumed as free surface allowing air bubbles freely leave the domain while slip boundary condition was applied for the liquid phase. The buoyant force in the current setup is the main driver of the flow, thus gravity is also included.

Simulation results of bubble void fraction, velocity and experimental velocity vector field are presented in figures 3-5. It can be seen that due to the lift and turbulence dispersion forces bubble column is smeared with reduction of maximum void fraction towards free surface. Bubbles near the sparger due to their high concentration effectively accelerate surrounding liquid, which leads to the turbulence intensification and formation of strong velocity gradients in the liquid phase. Both of that effects intensifies lateral forces, which, in turn, leads to significant smearing of the bubble column. Turbulence intensification can lead to the more intense diffusion of dissolved gas and, therefore, intensification of chemical processes.

Comparing the simulated (figure 4) and experimental (figure 5) velocity distributions, one can see that slight difference in gradient prediction exists, which is more pronounced in simulations. That can be dedicated to some uncertainties in experiment measurements since during LDA measurements nearby bubbles can alter measured data and due to the fact that experimental image was obtained from the averaging procedure over large period of time. Some discrepancies can also occur because of impact of the top boundary condition which didn't represent actual shape of water surface. However, the overall picture of the flow predicted correctly, with top recirculation zone close to the left wall and jet attachment point which lies 300 mm from the bottom wall.

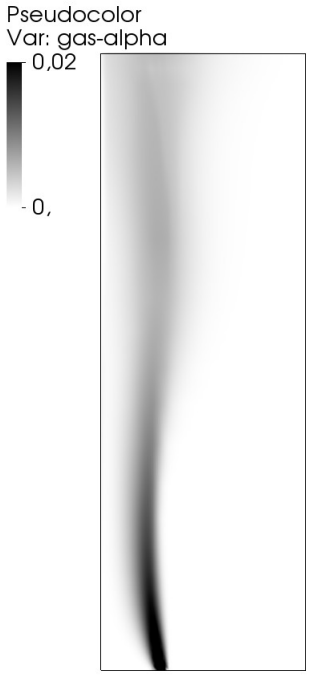

Figure 3. Bubble void fraction distribution in mid-plane obtained in simulation.

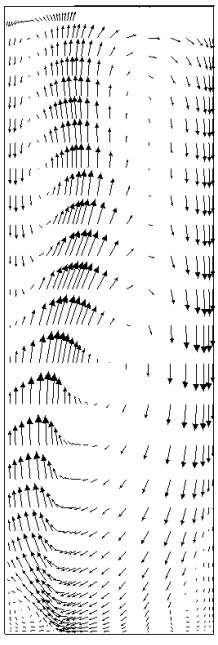

Figure 4. Liquid velocity vector field in mid-plane obtained in simulation, max value 0.24 m/s.

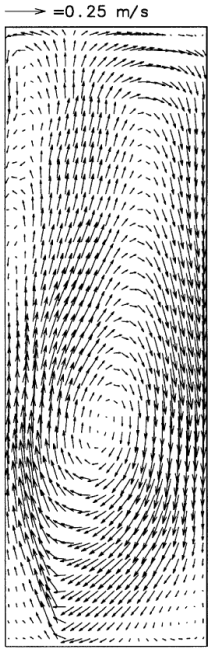

Figure 5. Experimental snapshot of the liquid velocity distribution in mid-plane.

5. Conclusion

The mathematical model based on the Euler-Euler approach and capable of description of polydisperse flows by the means of multi-class model was developed. The numerical algorithm was accordingly modified and numerical simulations were carried out for two distinctive cases of bubbly flows. It was proved that the proposed model and algorithm are able to correctly predict the flow structure under the real flow conditions, with qualitative and quantitative agreement with the available experimental data. Both downward flow inside straight pipe and upward bubbly flow inside rectangular bubble column were investigated, with comparison of velocity and bubble void fraction distributions.

References

[1] Chernyshev A, Kitanin E, Kumzerova E and Schmidt A 2007 *Proc. Int. Conf. on Multiph. Flow (Leipzig Germany)* Paper S7_Tue_D_29
[2] Iben U, Ivanov N, Isaenko I and Schmidt A 2015 *Tech. Phys. Lett.* **41**(12) 1159–62
[3] Chernyshev A and Schmidt A 2013 *AIP Conf. Proc.* **1558** 1071–4
[4] Loth E 2000 *Prog. Energy Comb. Sci.* **26** 161–223
[5] Yao W and Morel C 2004 *Int. J. Heat Mass Transfer* **47** 307–28
[6] Wang T, Wang J and Jin Y 2005 *Chem. Eng. Sci.* **60** 6199–209
[7] Bannari R, Kerdouss F, Selma B, Bannari A and Proulx P 2008 *Comp. and Chem. Eng.* **32** 3224–37
[8] Morel C, Ruyer P, Seiler N and Laviéville J M 2010 *Int. J. Multiph. Flow* **36** 25–39
[9] Chernyshev A S and Schmidt A A 2013 *Tech. Phys. Lett.* **39**(6) 548–51
[10] Lain S, Sommerfeld M, Broder D and Goz M 2002 *Int. J. Multiph. Flow* **28** 1381–407
[11] Tomiyama A, Tamai H, Zun I and Hosokawa S 2002 *Chem. Eng. Sci.* **57** 1849–58
[12] Patankar S V 1980 *Numerical Heat Transfer and Fluid Flow* (New York: McGraw-Hill)
[13] Ishii M, Paranjape S, Kim S and Sun X 2004 *Int. J. Multiph. Flow* **30** 779–801
[14] Sokolichin A and Eigenberger G 1999 *Chem. Eng. Sci.* **54** 2273–84